IEEE Photonics Journal
An IEEE Photonics Society Publication

Open Access

Strong Modulation Instability in a Silicon–Organic Hybrid Slot Waveguide

Volume 7, Number 4, August 2015

Xianting Zhang
Jinhui Yuan
Kuiru Wang
Zhe Kang
Binbin Yan
Xinzhu Sang
Qiang Wu
Chongxiu Yu
Gerald Farrell

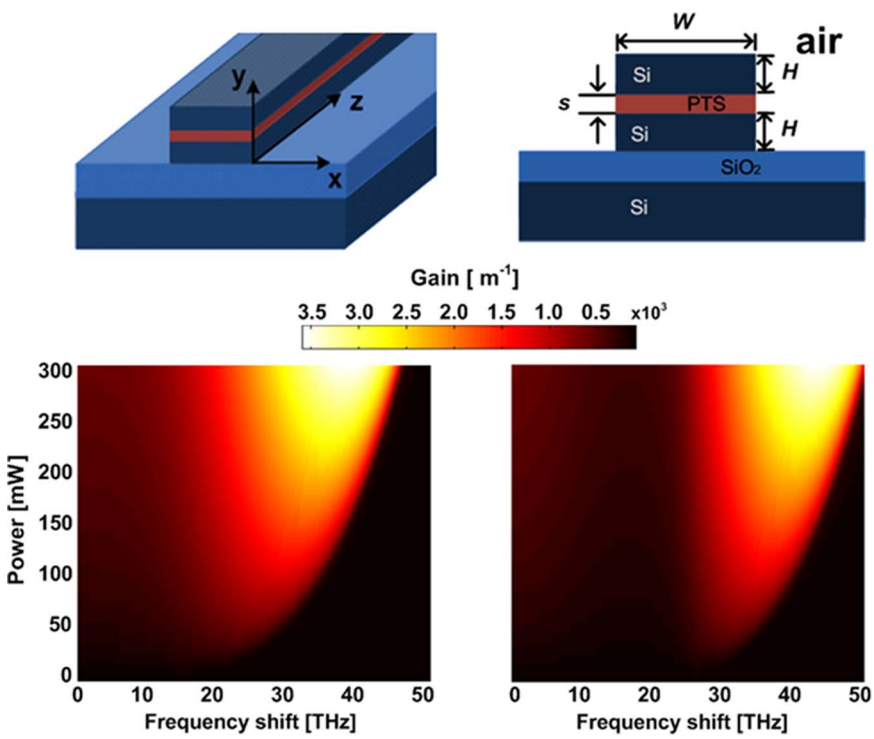

DOI: 10.1109/JPHOT.2015.2439952

Strong Modulation Instability in a Silicon–Organic Hybrid Slot Waveguide

Xianting Zhang,[1] Jinhui Yuan,[1,2] Kuiru Wang,[1] Zhe Kang,[1] Binbin Yan,[1] Xinzhu Sang,[1] Qiang Wu,[1,3] Chongxiu Yu,[1] and Gerald Farrell[4]

[1]State Key Laboratory of Information Photonics and Optical Communications, Beijing University of Posts and Telecommunications, Beijing 100876, China
[2]Photonics Research Center, Department of Electronic and Information Engineering, The Hong Kong Polytechnic University, Kowloon, Hong Kong
[3]Department of Physics and Electrical Engineering, Northumbria University, Newcastle upon Tyne NE1 8ST, U.K.
[4]Photonics Research Center, School of Electronic and Communications Engineering, Dublin Institute of Technology, Dublin, Ireland

DOI: 10.1109/JPHOT.2015.2439952

Manuscript received May 4, 2015; revised May 25, 2015; accepted May 28, 2015. Date of publication June 1, 2015; date of current version July 1, 2015. This work was supported in part by the National Natural Science Foundation of China under Grant 61307109 and Grant 61475023, by the Beijing Natural Science Foundation under Grant 4152037, by the National High-Technology Research and Development Program of China under Grant 2013AA031501, by the Specialized Research Fund for the Doctoral Program of Higher Education under Grant 20120005120021, by the Fundamental Research Funds for the Central Universities under Grant 2013RC1202, by the Fund of State Key Laboratory of Information Photonics and Optical Communications (BUPT) of China, by the Hong Kong Scholars Program 2013 under Grant PolyU G-YZ45, and by the Research Grant Council of the Hong Kong Special Administrative Region China under Grant PolyU5272/12E. Corresponding author: J. Yuan (e-mail: yuanjinhui81@163.com).

Abstract: In this paper, we investigate the strong modulation instability (MI) at telecommunication band in a silicon–organic hybrid slot waveguide. The organic material of polymer poly (bis para-toluene sulfonate) of 2, 4-hexadiyne 1, 6 diol (PTS), which has high third-order nonlinear refractive index and very low two-photon absorption, is used to fill the slot of the waveguide. The optical gain can be up to $\sim$3600 m^{-1} with a low pump peak power of 300 mW. By using Gaussian pulses with width of 10 ps and peak power of 250 mW, deep modulation of the pump is achieved, and the ultrashort pulse trains with the periods of 27 and 24 fs are obtained in the anomalous and normal group-velocity dispersion regions, respectively.

Index Terms: Modulation instability (MI), silicon–organic hybrid (SOH), slot waveguide, ultrashort pulse train.

1. Introduction

Silicon waveguides have been extensively studied because of its potential to satisfy the increasing demands on the electronics in optical communications. Benefiting from its good optical confinement, large nonlinear coefficient, and easy integration with the complementary metal-oxide semiconductor (CMOS), silicon waveguides are desirable in the realization of all-optical signal processing on the chip scale. Significant works on the on-chip optical devices have already been reported, including parametric amplifier [1]–[3], Raman laser [4]–[7], broadband wavelength converter [8]–[10], and analog-to-digital converter [11]. In addition, modulation instability (MI) in which a weak perturbation of the amplitude or phase of a continuous wave (CW) or

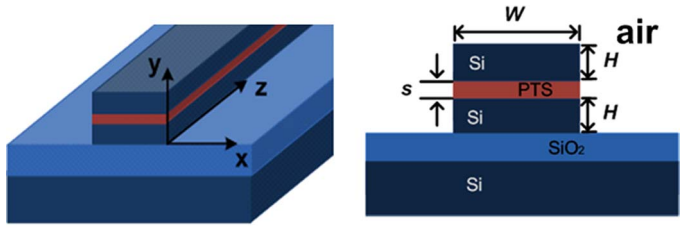

Fig. 1. (a) Three-dimensional structure of the proposed SOH waveguide and (b) the corresponding cross-section of the SOH waveguide. *W*: waveguide width; *s*: slot thickness; *H*: strip height.

quasi-CW wave grows exponentially, has been studied in the silicon-based waveguide [12], [13]. The MI process could induce deep modulations of an input CW or quasi-CW which could play an important role in the design of on-chip ultra-short pulse train source.

Nevertheless, for pure silicon waveguides, the MI process at telecommunication band is usually destroyed by the strong two-photon absorption (TPA) and free-carrier absorption (FCA) [13]. In recent years, silicon–organic hybrid (SOH) waveguides have emerged as an attractive optical structure because of its ability to overcome the TPA-induced intrinsic limitations in pure silicon waveguides. In a SOH waveguide, the silicon can be combined with other organic materials, which have a much higher third-order nonlinear refractive index and do not suffer from the TPA and FCA at the telecommunication band [14]–[16]. Meanwhile, the organic materials can be developed independent from the silicon-based waveguide which can induce remarkable nonlinear effects [15].

In this paper, we investigate the strong MI process in a horizontal slot-type SOH waveguide. The slot is filled with the organic material polymer poly (bis para-toluene sulfonate) of 2,4-hexadiyne 1, 6 diol (PTS). Simulation results show that a high optical gain is achieved with a low peak power pulse pump at telecommunication band and the ultra-short pulses, generated from deep modulation induced by MI, with periods of 27 and 24 fs are obtained in the anomalous and normal group-velocity dispersion (GVD) region, respectively. The proposed SOH waveguide is a good candidate for on-chip ultra-fast optical signal processing.

2. Design and Modeling

Here, the horizontal slot waveguide is chosen to avoid the processing difficulties encountered in slot filling or SiO_x etching [17], and it can be formed by the deposition or growth techniques with the nanometer-scale accuracy, which is critical to decrease the error caused by the fabrication of waveguide. Besides, it offers the advantages on a better control of layer thickness, and allows for much thinner slot layers [18]. This is better than a vertical slot that must be defined lithographically and etched down into a silicon waveguide [19], [20], which is difficult for a slot size below 50 nm. As shown in Fig. 1(a) and (b), the proposed SOH waveguide is with air cladding and the slot filled with PTS is sandwiched between two silicon strips. From the material dispersions of silicon, silicon dioxide, and PTS, the effective refractive index, n_{eff}, of the SOH waveguide is calculated using the full-vector finite element method (FEM), and the GVD (β_2), third-order (β_3), and fourth-order (β_4) dispersion parameters can be easily obtained through numerically differentiating the calculated n_{eff} since $\beta_{\mathrm{n}} = \mathrm{d}^{\mathrm{n}} n_{\mathrm{eff}}/\mathrm{d}\omega^{\mathrm{n}}$. The thickness of the slot and the width of the waveguide are $s = 20$ nm and $W = 540$ nm, respectively. Since the electric field discontinuity occurs at the horizontal interface for such a waveguide, the quasi transverse magnetic (TM) polarization [y direction as shown in Fig. 1(a)] should be used for the analysis. For different silicon strip heights, the GVD derived from the effective refractive index within the wavelength range of interest is shown in Fig. 2. It shows that the ideal strip height is determined to be 470 nm because the zero GVD wavelength is very close to 1550 nm.

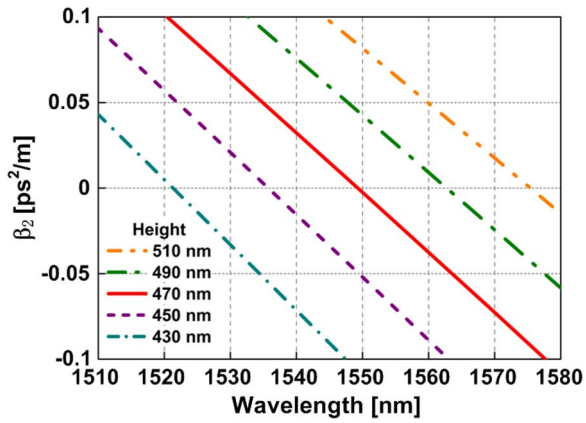

Fig. 2. GVD of the waveguide calculated for different heights of the silicon strip.

The nonlinear index of the organic material PTS is $n_2 = 2.2 \times 10^{-16}\text{m}^2\text{W}^{-1}$, which is nearly two order of magnitude higher than that of silicon [14], [21], [22]. The peak of the TPA in the PTS is located at 930 nm which decreases monotonically with increasing wavelength and reaches very low value at telecommunication band [14], [16]. Hence the proposed SOH waveguide could induce a much higher nonlinear effects without suffering from the TPA and the associated FCA at telecommunication band. The dynamics of optical wave propagating in the proposed SOH waveguide is governed by the nonlinear Schrödinger equation [12]–[14] as

$$i\frac{\partial A}{\partial z} + \sum_{k=2}^{4} \frac{(i)^k \beta_k}{k!} \frac{\partial^k A}{\partial t^k} + \gamma |A|^2 A + i\frac{\alpha}{2} A = 0 \tag{1}$$

where A, β_κ, γ, and α represent the slowly varying pulse envelop, kth-order dispersion parameter, nonlinear coefficient, and linear loss, respectively. Here we consider the chromatic dispersion of the SOH waveguide up to the fourth-order. We found that inclusion of higher order dispersion did not have significant effect on the simulation results. To analyze the MI process we start from the steady-state solution

$$A_0 = \sqrt{P_0} \exp\left[i(\gamma P_0 - \alpha/2)z\right] \tag{2}$$

where P_0 is the peak power of the input pump. We consider a small perturbation of the steady-state solution $A_\text{p} = A_0 + \delta A$. Here δA is assumed to be

$$\delta A = \mu(z) \exp\left[i(Kz - \Omega t)\right] + \nu(z) \exp\left[-i(Kz - \Omega t)\right] \tag{3}$$

where $\mu(z)$ and $\nu(z)$ are the complex perturbation amplitudes corresponding to the Stokes and anti-Stokes sidebands. The parameters K and Ω are the wave number and frequency offset of the small perturbation, respectively. Substituting A_p into (1), the equation for the perturbed field $\mathbf{Y} = [\mu(z), \nu(z)]^\text{T}$ is given by

$$\begin{aligned} \frac{d\mathbf{Y}}{dz} &= i\mathbf{M}\mathbf{Y} \\ &= i \begin{bmatrix} \sum_{k=2}^{4} \frac{\beta_k \Omega^k}{k!} - K + \gamma P_0 + i\frac{\alpha}{2} & \gamma P_0 \\ -\gamma P_0 & -\sum_{k=2}^{4} \frac{\beta_k (-\Omega)^k}{k!} - K - \gamma P_0 - i\frac{\alpha}{2} \end{bmatrix} \begin{bmatrix} \mu(z) \\ \nu(z) \end{bmatrix} \end{aligned} \tag{4}$$

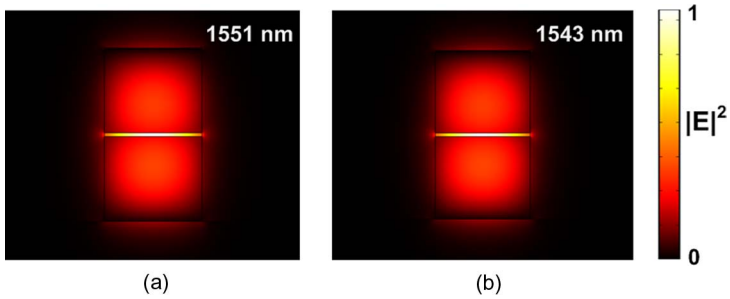

Fig. 3. Calculated transverse profiles of the electric field for quasi-TM polarization at (a) 1551 nm and (b) 1543 nm.

where **M** is the MI matrix. By considering the nontrivial solutions, the relationship between K and Ω is calculated as

$$K = \frac{\beta_3\Omega^3}{6} \pm \frac{1}{2}\left[\left(\beta_2\Omega^2 + \frac{\beta_4\Omega^4}{12}\right)^2 + 4\left(\beta_2\Omega^2 + \frac{\beta_4\Omega^4}{12}\right)\left(\gamma P_0 + i\frac{\alpha}{2}\right) + i\alpha(4\gamma P_0 + i\alpha)\right]^{\frac{1}{2}} \quad (5)$$

when K possesses a nonzero imaginary part, the perturbation grows exponentially with z and the MI is measured by the power gain defined as $G(\Omega) = 2|\mathrm{Im}[K(\Omega)]|$. We note that even in the normal dispersion region, the presence of the fourth-order dispersion β_4 could render a nonzero imaginary part of K and thus induce the MI if the value of β_2 is sufficiently small [12], [13]. Also, since the first term on the right-hand side of (5) is always real, the third-order dispersion plays no role in the MI process.

3. Simulation Results and Discussions

The MI process is studied in both the anomalous and normal dispersion region. A 10 ps Gaussian pulse at 1551 nm, which is used as the quasi-CW steady-solution, is launched into the SOH waveguide when studying the MI in the anomalous dispersion region, and for the normal dispersion region, the same pulse at 1543 nm is used instead. Fig. 3(a) and (b) shows the calculated transverse profiles of the electric field for quasi-TM polarization in both cases. We observed that most of the electric field is confined inside the low-index slot, hence the light confined in the slot could propagate without severe impairment by the TPA in PTS. The intense of the light propagating outside the slot is quite small since the electric field in large cross-section silicon strips is far more weaker. Consequently, the induced TPA and FCA in the silicon strips could be neglected when compared to the linear loss of the waveguide, which is approximately 4.5 dB/cm [14], [16]. The calculated dispersion parameters for the anomalous are $\beta_2 = -4.65\times10^{-3}$ ps^2/m, $\beta_3 = 4.62\times10^{-3}$ ps^3/m, and $\beta_4 = -1.17\times10^{-5}$ ps^4/m, and for the normal dispersion regions are and $\beta_2 = 0.0204$ ps^2/m, $\beta_3 = 4.41\times10^{-3}$ ps^3/m and $\beta_4 = -1.10\times10^{-5}$ ps^4/m. Fig. 4(a) and (b) shows the obtained MI gain spectra as the function of the pump peak power in anomalous and normal dispersion region, respectively. The corresponding 2-D gain profiles are shown in Fig. 4(c) and (d). The negative part of the gain profiles are not shown here because of the symmetry of the curves. It is evident that the optical gains in both the anomalous and normal dispersion regions increases when P_0 increases. For $P_0 = 300$ mW, the optimum frequency offset $(\mathrm{d}G(\Omega)/\mathrm{d}\Omega = 0)$ in the anomalous and normal dispersion regions are given by $\Omega_p/2\pi = 38.2$ and 43.3 THz, respectively. The strong MI gain of $\sim$3600 m^{-1} in both cases could be achieved by utilizing a pump with a low peak power. The results obtained here represent a substantial improvement over those reported previously for the MI process. In the previous work [13], the MI gain was only less than 600 m^{-1} when the input peak power is 3 W. In another experiment [23], the signal got a gain of less than 50 dB in a 2-cm-long silicon photonic wire with a peak power of 13.5 W for the

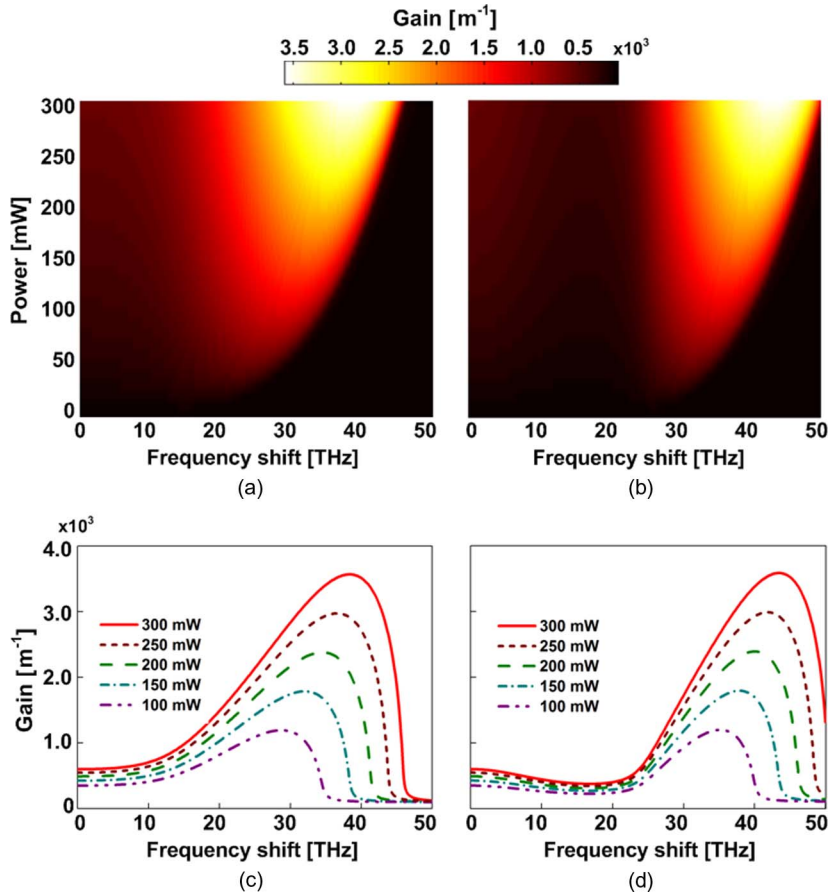

Fig. 4. MI gain spectra as a function of the input peak powers for (a) the anomalous and (b) normal dispersion regions. (c) and (d) Two-dimensional gain profiles corresponding to (a) and (b), respectively.

presence of the MI. Here, we would like to highlight that even if at the pump power $P_0 = 100$ mW, the optical gain obtained in our work is above 1000 m^{-1} as seen from Fig. 4(c) and (d), which is still outstanding compared to other works. These remarkable results are due to the negligible TPA and large nonlinear coefficient, calculated to be up to 5400 $W^{-1}m^{-1}$, in the designed slot type SOH waveguide. From Fig. 4(c) and (d) Ω_p changes by nearly 2 THz when P_0 is changed by 50 mW. Thus Ω_p is tunable by varying P_0.

As a result of the MI process, the deep femtosecond modulation of the pump pulse in the proposed SOH waveguide is studied. The temporal profiles of pulses for different propagation distances are shown in Fig. 5. The results are obtained by using a 250 mW pump pulse together with the perturbation with the optimum frequency offset, which is more than 1000 times weaker than the pump. It is evident that the deep modulations can be achieved in both anomalous and normal GVD regions. As depicted in Fig. 5(a) and (c), the weak perturbation undergoes a dramatic amplification owing to the presence of the strong MI process in the SOH waveguide during the propagation. It is shown that the pulses exhibit an obvious oscillatory tail after the propagation distance of 3 mm. This is caused by the third-order dispersion since the pump pulses are located near the zero GVD wavelength. Fig. 5(b) and (d) shows the zoom-in figures of Fig. 5(a) and (c), respectively. The deep femtosecond modulations with the period of 27 and 24 fs are found in anomalous and normal dispersion regions, respectively. The results agree well with the gain spectra as shown in Fig. 4 because the frequency offset in the normal dispersion region is larger than that in the anomalous dispersion region for the same pump pulses.

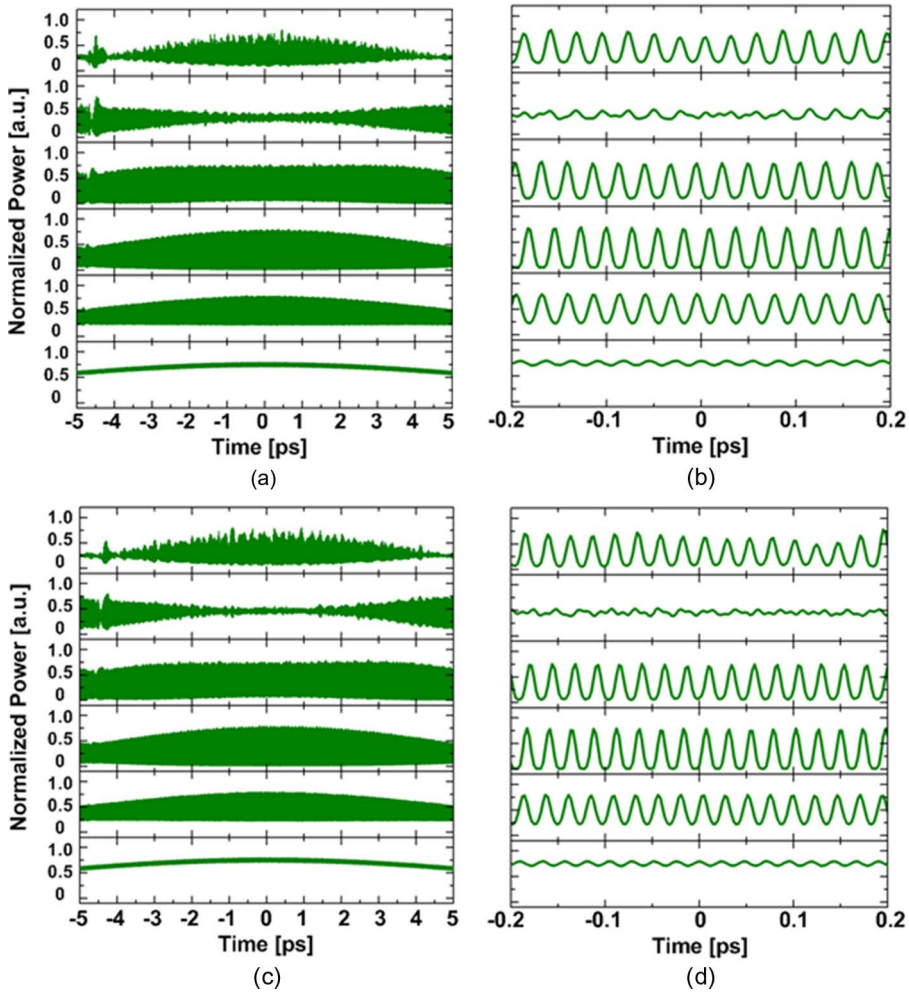

Fig. 5. (a) Whole pulse shapes at different propagation distances in A, (b) the zoom-in figure of (a) from −0.2 to 0.2 ps, and (c) and (d) the same results corresponding to B. The propagation distances are $z = 0$, 2, 3, 4, 5, and 6 mm, respectively (from the bottom to the top).

The period of the pulses does not show an obvious change with the increasing propagation distance because they depend on the frequency offset of the perturbations. The finding could play an important role in the design of the ultra-short pulse train source since it generated the ultra-short pulses on the chip scale and at the repetition rates higher than those attainable from mode-lock lasers [24]–[26]. The pulse train generated could be very useful and contribute to a better performance in ultra-fast optical signal processing, e.g., the FWM based optical sampling [27], [28] and Optical demultiplexing [29]. Nevertheless, the uniformity, which apparently influence the applications of the pulse trains, is found to not always be perfect, as depicted in these figures. It changes with the increasing propagation distance and becomes the best when the propagation distance of the pulses reaches 4 mm. However, it becomes much worse as the propagation distance further increases. As shown in Fig. 5(a) and (c), the pulse trains takes on an obvious variation after 4 mm, and the main reason is considered to be the modulation effect induced by the low frequency components. This means the optical components with lower frequency shifts can also be amplified by the nonlinear effects. The new frequencies components are created by the interaction of higher order dispersion and the nonlinear effect which results in resonant radiation [30], [31]. In addition, P_0 will be reduced by the linear loss of SOH waveguide. From Fig. 4 the optical components at lower frequency away from Ω_p will be amplified,

which may also induce a large variation of the pulse train. Therefore, the propagation distance should be optimized so as to minimize the distortion induced by the third-order dispersion and other linear or nonlinear processes mentioned above. In our work, the optimal propagation distance is chosen to be 4 mm.

4. Conclusion

In summary, we investigate the strong MI process at telecommunication band in a SOH slot waveguide. The light is confined in the low-index slot which is filled with the organic material PTS. Because of its high third-order nonlinear refractive index and negligible TPA, an optical gain of $\sim$3600 m^{-1} can be achieved when the pump pulses with the peak power of 300 mW are used. We also show that the deep modulations with the period of 27 and 24 fs can be achieved and generate an ultra-short pulse train by using Gaussian pulses with a pulse width of 10 ps and peak power of 250 mW in the anomalous and normal GVD regions, respectively. The proposed device can find important application in the on-chip ultra-fast all-optical signal processing.

References

[1] M. A. Foster *et al.,* "Broad-band optical parametric gain on a silicon photonic chip," *Nature.*, vol. 441, no. 7096, pp. 960–963, May 2006.

[2] S. Lavdas *et al.,* "Wavelength conversion and parametric amplification of optical pulses via quasi-phase-matched four-wave mixing in long-period Bragg silicon waveguides," *Opt. Lett.*, vol. 39, no. 13, pp. 4017–4020, Jul. 2014.

[3] Y. Zhang *et al.,* "Performance analysis of dual-pump optical parametric amplifiers in silicon waveguide," *Opt. Commun.*, vol. 283, no. 15, pp. 3043–3048, Aug. 2010.

[4] H. Rong *et al.,* "A continuous Raman silicon laser," *Nature.*, vol. 433, pp. 725–728, Jan. 2005.

[5] H. Rhee *et al.,* "Operation of a Raman laser in bulk silicon," *Opt. Lett.*, vol. 36, no. 9, pp. 1644–1646, May 2011.

[6] F. De Leonardis, B. Troia, and V. M. N. Passaro, "Design rules for Raman lasers based on SOI racetrack resonators," *IEEE Photon. J.*, vol. 5, no. 6, Dec. 2013, Art. ID. 1502431.

[7] Y. Huang, P. Shum, and C. Lin, "Proposal for loss reduction and output enhancement of silicon Raman laser using bi-directional pumping scheme," *Opt. Commun.*, vol. 283, no. 7, pp. 1389–1393, Apr. 2010.

[8] X. Zhang *et al.,* "Enhanced broadband parametric wavelength conversion in silicon waveguide with the multi-period grating," *IEEE Photon. J.*, vol. 6, no. 6, Dec. 2014, Art ID. 6601410.

[9] Y. Huang *et al.,* "Wavelength conversion bandwidth enhancement through quasi-phase-matching in a width modulated silicon waveguide," presented at the Opt. Fiber Commun. Conf./Nat. Fiber Optic Eng. Conf., Mar. 17–21, 2013, Paper JTh2A.33.

[10] Y. Okawachi, A. L. Gaeta, and M. Lipson, "Breakthroughs in nonlinear silicon photonics 2011," *IEEE Photon. J.*, vol. 4, no. 2, pp. 600–606, Apr. 2012.

[11] Z. Kang *et al.,* "CMOS-compatible 2-bit optical spectral quantization scheme using a silicon-nanocrystal-based horizontal slot waveguide," *Sci. Rep.*, vol. 4, p. 7177, Nov. 2014.

[12] N. C. Panoiu, X. Chen, and R. M. Osgood, Jr., "Modulation instability in silicon photonic nanowires," *Opt. Lett.*, vol. 31, no. 24, pp. 3609–3611, Dec. 2006.

[13] L. M. Mandeng and C. Tchawoua, "Impact of input profile, absorption coefficients, and chirp on modulational instability of femtosecond pulses in silicon waveguides under fourth-order dispersion," *J. Opt. Soc. Amer. B.*, vol. 30, no. 5, pp. 1382–1391, May 2013.

[14] L. An, H. Liu, Q. Sun, N. Huang, and Z. Wang, "Wavelength conversion in highly nonlinear silicon–organic hybrid slot waveguides," *Appl. Opt.*, vol. 53, no. 22, pp. 4886–4893, Aug. 2014.

[15] C. Koos *et al.,* "All-optical high-speed signal processing with silicon–organic hybrid slot waveguides," *Nat. Photon.*, vol. 3, pp. 216–219, Apr. 2009.

[16] S. Polyakov, F. Yoshino, M. Liu, and G. Stegeman, "Nonlinear refraction and multiphoton absorption in polydiacetylenes from 1200 to 2200 nm," *Phys. Rev B.*, vol. 69, no. 11, Mar. 2004, Art. ID. 115421.

[17] E. Jordana *et al.,* "Deep-UV lithography fabrication of slot waveguides and sandwiched waveguides for nonlinear applications," in *Proc. 4th IEEE Int. Conf. Group IV Photon.*, 2007, pp. 1–3, ThC3.

[18] K. Preston and M. Lipson, "Slot waveguides with polycrystalline silicon for electrical injection," *Opt. Express*, vol. 17, no. 3, pp. 1527–1534, Feb. 2009.

[19] V. R. Almeida, Q. Xu, C. A. Barrios, and M. Lipson, "Guiding and confining light in void nanostructure," *Opt. Lett.*, vol. 29, no. 11, pp. 1209–1211, Jun. 2004.

[20] Q. Xu, V. R. Almeida, R. R. Panepucci, and M. Lipson, "Experimental demonstration of guiding and confining light in nanometer-size low-refractive-index material," *Opt. Lett.*, vol. 29, no. 14, pp. 1626–1628, Jul. 2004.

[21] L. Yin and G. P. Agrawal, "Impact of two-photon absorption on self-phase modulation in silicon waveguides," *Opt. Lett.*, vol. 32, no. 14, pp. 2031–2033, Jul. 2007.

[22] H. K. Tsang *et al.,* "Optical dispersion, two-photon absorption and self-phase modulation in silicon waveguides at 1.5 mm wavelength," *Appl. Phys. Lett.*, vol. 80, no. 3, pp. 416–418, Jan. 2002.

[23] B. Kuyken *et al.,* "50 dB parametric on-chip gain in silicon photonic wires," *Opt. Lett.*, vol. 36, no. 22, pp. 4401–4403, Nov. 2011.

[24] G. P. Agrawal, *Nonlinear Fiber Optics*, 4th ed. San Diego, CA, USA: Academic, 2007.
[25] S. Jyu *et al.,* "250-GHz passive harmonic mode-locked Er-doped fiber laser by dissipative four-wave mixing with silicon-based micro-ring," *IEEE Photon. J.*, vol. 5, no. 5, Oct. 2013, Art. ID. 1502107.
[26] X. Li *et al.,* "Wavelength-switchable and wavelength-tunable all-normal-dispersion mode-locked Yb-doped fiber laser based on single-walled carbon nanotube wall paper absorber," *IEEE Photon. J.*, vol. 4, no. 1, pp. 234–241, Feb. 2012.
[27] C.-S. Bres, N. Alice, A. H. Gnauck, R. M. Jopson, and S. Radic, "Multicast parametric synchronous sampling," *IEEE Photon. Technol. Lett.*, vol. 20, no. 14, pp. 1222–1224, Jul. 2008.
[28] X. Zhang *et al.,* "Scheme for multicast parametric synchronous optical sampling," *Opt. Eng.*, vol. 53, no. 5, May 2014, Art. ID. 056102.
[29] C.-S. Brès *et al.,* "Optical demultiplexing of 320Gb/s to 8×40 Gb/s in single parametric gate," *J. Lightw. Technol.*, vol. 28, no. 4, pp. 434–442, Feb. 2010.
[30] S. Roy, S. K. Bhadra, and G. P. Agrawal, "Effects of higher-order dispersion on resonant dispersive waves emitted by solitons," *Opt. Lett.*, vol. 34, no. 13, pp. 2072–2074, Jul. 2009.
[31] J. Peng, F. Zhu, F. Benabid, and A. V. Sokolov, "Carrier-envelope offset frequency measurement for tunable femto-second lasers using resonant dispersive waves," *Opt. Lett.*, vol. 36, no. 6, pp. 891–893, Mar. 2011.